Journal of Materials Chemistry C

Accepted Manuscript

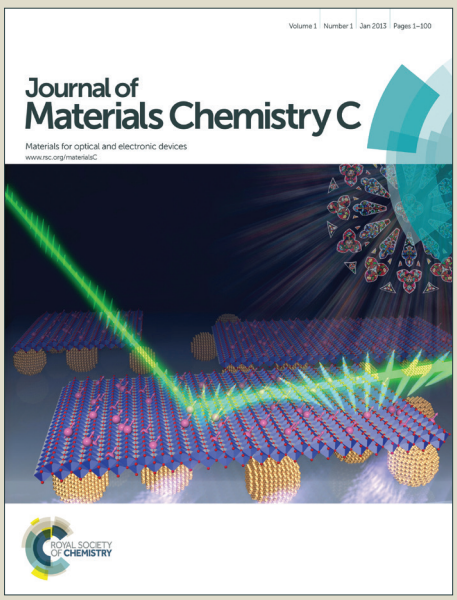

ROYAL SOCIETY OF CHEMISTRY

www.rsc.org/materialsC

Multicolor upconversion $NaLuF_4$ fluorescent nanoprobe for plant cell imaging and detection of Sodium fluorescein

Zenghui Chen,[a] Xiaofeng Wu,*[b] Shigang Hu,[b] Pan Hu,[b] Huanyuan Yan,[c] Zhijun Tang,[b] Yunxin Liu*[a]

a Department of Physics and Electronic Science, b School of Information and Electrical Engineering, c College of Mechanical and Electrical Engineering, Hunan University of Science and Technology, Xiangtan 411201, China

**E-mail:* lyunxin@163.com; xfwuvip@126.com

Multicolor upconversion $NaLuF_4$ nanocrystals with strong upconversion luminescence and biocompatibility were synthesized by a general solvothermal method and subsequent surface modification. The emission color of these $NaLuF_4$ upconversion nanoparticles can be easily modulated by the doping. These multicolor $NaLuF_4$ upconversion nanorystals can be employed as fluorescent probes for in vivo biological imaging without the need of slicing process for living beings. Importantly, the upconversion nanoprobes (UCNPs) with an acidic ligand can quickly capture the basic sodium fluorescein (SF) in plant cells and forms a close UCNPs@SF system. The UCNPs@SF system can emit cyan light due to luminescence resonant energy transfer (LRET) from UCNPs to SF under the excitation of 980 nm infrared light, which is actually composed of the blue emission of $NaLuF_4$:18%Yb^{3+}/0.5%Tm^{3+} nanoprobes and the green emission of SF. The concentration of SF can be easily addressed according to the Integral Intensity Ratio of Green to Blue fluorescent signals (IIRGB). The detection limitation of sodium fluorescein for this upconversion fluorescent nanoprobe can reach to 0.14 μg/cm^3 in plant cell.

1. Introduction

The fluorescent labeling has wide application for imaging the biological tissue and cell units at different wavelength, by which the complex biological process inside the cells or between cells can be observed more clearly, distinguished more accurately and avoid the slicing process compared with the conventional biological imaging.[1-7] The fluorescent labels with high sensitivity, natural affinity, well stability and sharp emission band are very desirable for high precise detection or cell imaging in vivo or in vitro.[8-10] In recent years, there is increasing interest in developing novel materials with high fluorescent signal to noise ratio for cell imaging and tracing metal ions or organic chemicals in vivo.[11-12] Conventional organic dyes and fluorescent protein have applied for imaging cells and tissues already.[13-15] Unfortunately, there are some intrinsic shortcomings limiting their ability for long-term and high-resolution imaging, for example, the strong photo-bleaching existed when used in cell imaging; the broad emission band of organic fluorephores could not be well coded for multicolor biological labeling; their rapid metabolic degradation and photo degradation are unsuitable for long time cell monitoring.[16,17] Semiconductor quantum dots

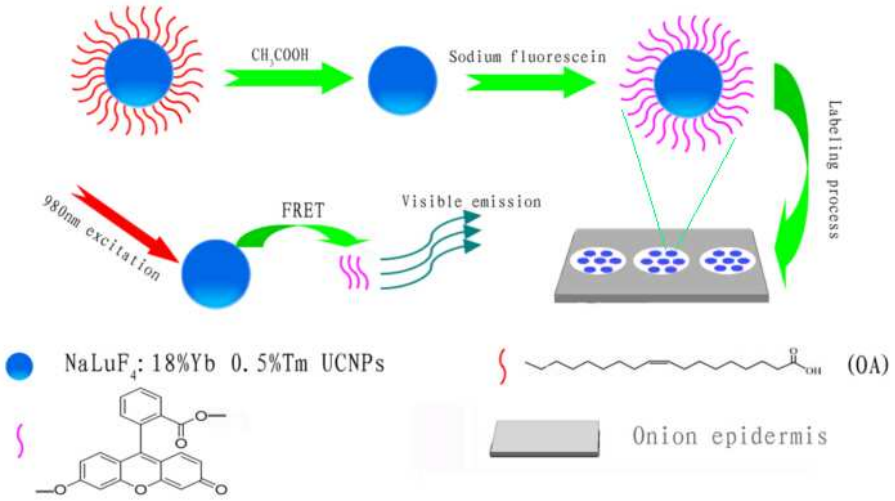

Scheme 1 Schematic illustration of LRET-based detection of sodium fluorescein using UCNPs as probes.

(such as CdS, CdTe) have also developed for a new generation probe for optical labeling and cell imaging.[18,19] Though QDs possess high quantum yield, broad ultraviolet (UV) excitation, narrow size-dependent tunable emission bandwidth, high photostability, and long fluorescence lifetime, their potential toxicity and chemical instability are intrinsic defects for achieving stable and innocuous cell imaging and clinical applications.[20-23] In addition, both organic dyes and QDs are excited by UV and visible light, which often induced inevitable background autofluorescence from biological tissues, which leads to low signal to noise ratios. To overcome these drawbacks of organic dyes and QDs, advanced upconversion nanoparticle probes are developed and receive increasing attention.[24,25]

Upconversion luminescence (UCL) is a process where low energy photons (infrared light) is always converted into higher energy ones (visible light) by sequential absorption of two photons or multiphoton. Upconversion nanoparticles have many conceivable advantages compared with conventional dyes and quantum dots, such as greater tissue penetration of infrared excitation, intense visible emission, complete absence of autofluorescence from biological tissue, high signal to noise ratio, large Stokes shift, resulting in their increasing application in cell imaging and clinical therapy.[26-28] To date, upconversion nanocrystals with surface modification have been widely reported in HeLa cell imaging in vitro, living mouses imaging in vivo, and in monitoring the lymph nodes, tumors, and chemical analytes.[17,29-31]

In this work, we focus on application of the multicolor upconversion nanoparticles in onion epidermal cell imaging and detection of sodium fluorescein in onion epidermal cell.[32,33] A series of $NaLuF_4$ nanocrystals with controlled particle size and intense luminescence were synthesized via a facile solvent-thermal method, which can emit six different color under a 980 nm laser excitation by varying dopant concentration.[34] Multicolor UCL imaging is demonstrated by labeling onion epidermal cells with these synthesized nanoparticles. On the other hand, we developed an upconversion LRET-based nano-system composed of $NaLuF_4$:18%Yb^{3+}/0.5%Tm^{3+} UCNPs and sodium fluorescein (UCNPs@SF), where sodium fluorescein can emit green light by absorbing blue emission from $NaLuF_4$:18%Yb^{3+}/0.5%Tm^{3+} nanoprobes

under excitation of 980 nm laser, as shown in Scheme 1. The IIRGB signal is measured for accurately detecting the concentration of sodium fluorescein in the onion epidermal cell by a convenient and fast manner without the interference of photobleaching and autofluorescence.[35] The LRET-based UCNPs@SF system can be extended for detecting other organic dyes and fluorescent proteins in living beings in vivo.

2. Experimental

$LuCl_3$•$6H_2O$ (99.9%), $YbCl_3$•$6H_2O$ (99.9%), $TmCl_3$•$6H_2O$ (99.9%), $ErCl_3$•$6H_2O$ (99.9%), NaOH (98+%), NH_4F (98+%), methanol (99.5%), 1-Octadecene (ODE) (90%), oleic acid (OA) (90%), sodium fluorescein, were purchased from Sigma Aldrich. Deionized water was used throughout. Unless otherwise noted, all chemicals were used directly without further purification.

2.1 Synthesis of $NaLuF_4$ nanoparticles

In a typical procedure for the synthesis of $NaLuF_4$:Yb^{3+},Er^{3+}/Tm^{3+} nanoparticles, 2 mL water solution of $RECl_3 \cdot 6H_2O$ (0.2 M, RE= Lu, Yb and Er/Tm) was added to a 50 mL flask containing ODE (12 ml) and OA (4 ml). The resulting mixture was heated to 160 °C with constant stirring to remove residual water and oxygen. After 30 min, the temperature was cooled to room temperature with general flow of argon gas through the reaction flask. Shortly thereafter, 5 ml methanol solution of NH_4F (1.5 mmol) and NaOH (1 mmol) was added and the resultant solution was stirred for another 30 min under 50 °C of temperature. After the methanol from the reaction mixture was evaporated, the solution was heated to 310 °C under an argon atmosphere for 60 min and then cool down to room temperature naturally. The resulting nanoparticles were precipitated by addition of ethanol, collected by centrifugation at 10000 rpm for 5 min, washed with ethanol three times, finally these prepared nanocrystals could be re-dispersed in nonpolar organic solvent such as cyclohexane and chloroform.

2.2 Characterization

The size and morphology of the prepared nanoparticles were measured using a H-7650c transmission electron microscopy (TEM) operating at 80 kV and a JEM 3010 high-resolution transmission electron microscopy operating at 200 kV (HRTEM). The photoluminescence (PL) emission spectra was measured from 400 to 700 nm using a Hitachi F-2700 spectrophotometer equipped with a 980 nm laser as the excitation source. The photo of upconversion luminescence was obtained digitally by a Sony multiple CCD camera.

Imaging of the nanoparticle uptook by onion epidermal cells was carried out using Olympus BX43 fluorescence microscopy under the excitation of a NIR 980 nm laser. The power density was 100 mW/cm^2 in front of lens. The multicolor fluorescence was collected by a Tucsen H-694CICE digital camera. All studies were carried out at room temperature.

3. Results and discussion

3.1 Upconversion fluorescence properties of $NaLuF_4$ nanoparticles

A solvothermal method was employed to synthesize $NaLuF_4$ nanocrystals with controlled particle size. Dopants play a major role in controlling the size and shape of $NaLuF_4$ nanoparticles. To reveal the morphology and size control, the synthesized $NaLuF_4$ nanocrystals were characterized by using TEM and high resolution TEM (HRTEM) as shown in Fig. 1. From these TEM images, all eight kinds of as-prepared nanoparticles appear almost spherical in shape

and monodisperse. The average diameters of the prepared $NaLuF_4$ nanoparticles doped with $18\%Yb^{3+}/0.5\%Tm^{3+}$, $18\%Yb^{3+}/0.04\%Er^{3+}/0.7\%Tm^{3+}$, $18\%Yb^{3+}/2\%Er^{3+}$, (30,32,50,70,90%) $Yb^{3+}/1\%Er^{3+}$ are determined to be about 40±2.6, 600±3.1, 50±1.4, 20±1.0, 30±1, 25±5.2, 7±0.4, 30±2.4 nm, respectively. As shown in Fig. 1b, it can be seen that the uniform hexagonal particles with lager diameter could be obtained by co-doping Er^{3+} and Tm^{3+}. With the increase of the dopant concentration of Yb^{3+} from 30% (Fig. 1d) to 32% (Fig. 1e), the diameter of $NaLuF_4$ nanoparticles increased from ~20 nm to ~30 nm. It is summarized that the Lu^{3+} ions (r=1.117 Å) in $NaLuF_4$ host lattice have been substituted partly by the slight lager lanthanide ions Yb^{3+} (r=1.125 Å), then the size of the prepared nanocrystals becomes lager than before when controlling over other experimental variables.[36] However, increasing the concentration of Yb^{3+} from 32% to 70% (Fig. 1e-g), the corresponding diameter decreased. Actually, the samples doped with 32% to 70% Yb^{3+} ion are solid solution composed of $NaLuF_4$ and $NaYbF_4$ crystal phase. The competition exists in the nucleation and growth of $NaLuF_4$ and $NaYbF_4$ crystals. It can be inferred from Fig. 1e-f that the nucleation and growth competition between $NaLuF_4$ and $NaYbF_4$ crystals reaches an equivalent value for the sample with 70% Yb^{3+} so that the smallest particles formed with uniform particle size. Further increasing the content of Yb^{3+} to 90%, this equivalence was destroyed and almost pure $NaYbF_4$ crystal phase formed, accompanied with an increase in particle size (see Fig. 1h). These uniform nanoparticles display regular morphology and high crystal quality. Typical high resolution transmission electron microscopy of (Figure 1e, inset) shows the distance between the lattice fringes of 0.32 nm along (0001)

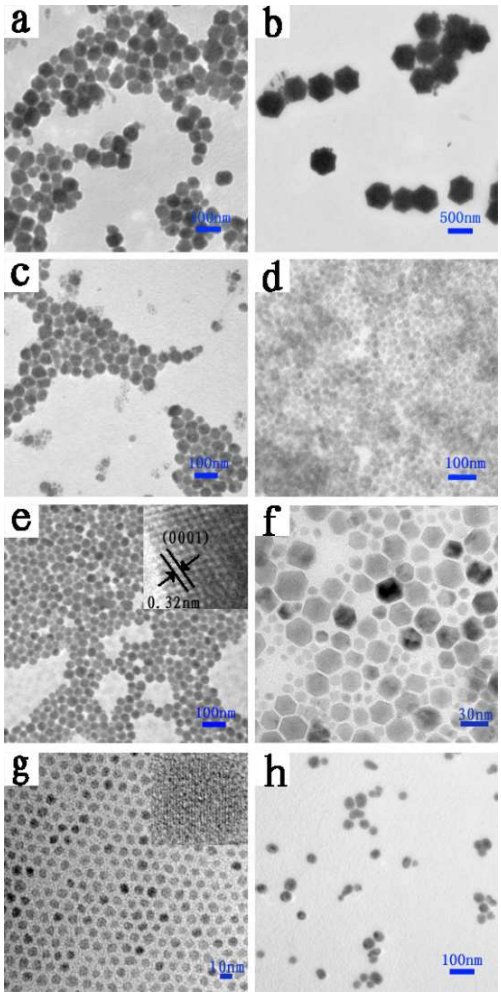

Fig. 1 TEM images of $NaLuF_4$ nanoprobes doped with (a) $18\%Yb^{3+}/0.5\%Tm^{3+}$; (b) $18\%Yb^{3+}/0.04\%Er^{3+}/0.7\%Tm^{3+}$; (c) $18\%Yb^{3+}/2\%Er^{3+}$; (d-h) $(30,32,50,70,90\%)Yb^{3+}/1\%Er^{3+}$. The insets of (e) and (g) show the corresponding high-resolution TEM image.

orientation in the $NaLuF_4$ nanocrystals, which also revealed their highly crystalline nature and structural uniformity.

The upconversion luminescence spectra of $Yb^{3+}/Er^{3+}/Tm^{3+}$ co- or tri-doped $NaLuF_4$ nanoparticle were measured under 980 nm diode laser excitation and shown in Fig. 2 and Fig. 3. The luminescence spectrum of $NaLuF_4$:$18\%Yb^{3+}$,$0.5\%Tm^{3+}$ (Fig. 2a) shows two sharp emission bands centered at 452 nm and 479 nm which can be assigned to the Tm^{3+}-$4f^n$ electronic transitions $^1D_2 \rightarrow {}^3F_4$ and $^1G_4 \rightarrow {}^3H_6$, respectively, and show blue light as

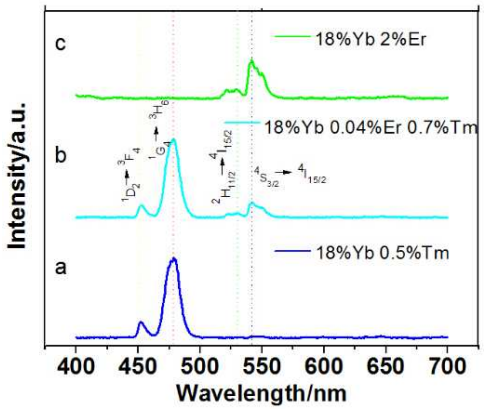

Fig. 2 Room-temperature upconversion fluorescent spectra of $NaLuF_4$ doped with (a) 18%Yb^{3+}/0.5%Tm^{3+}, (b) 18%Yb^{3+}/0.04%Er^{3+}/0.7%Tm^{3+}, (c) 18%Yb^{3+}/2%Er^{3+} under the excitation of a 980 nm laser diode.

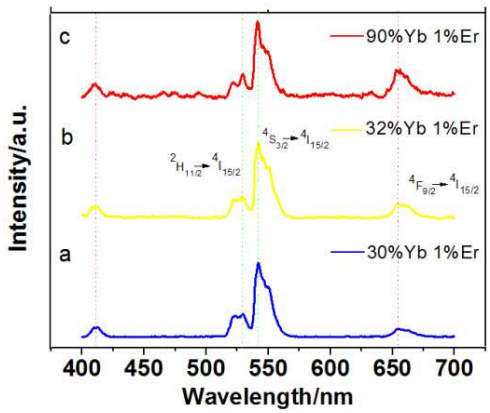

Fig. 3 Room-temperature upconversion fluorescent spectra of $NaLuF_4$ doped with (30,32,90)%Yb^{3+}/1%Er^{3+} under the excitation of a 980 nm laser diode.

a whole to naked eyes (Fig. 4b). For Yb^{3+}/Er^{3+}/Tm^{3+} tri-doped $NaLuF_4$ nanoparticles (Fig. 2b), the strongest blue emission peak at 479 nm is ascribed to the $^1G_4 \rightarrow {}^3H_6$ transition of Tm^{3+}, while the green emission peaks at 529 nm and 541 nm are attributed to $^2H_{11/2} \rightarrow {}^4I_{15/2}$ and $^4S_{3/2} \rightarrow {}^4I_{15/2}$ transition of Er^{3+} ions, respectively, and show cyan light to naked eyes as a whole (Fig. 4c). Fig. 2c shows the upconversion luminescence spectrum of $NaLuF_4$: 18%Yb^{3+}/2%Er^{3+} nanocrystal, the dominant green emission peaks at 529 nm and 541 nm can be assigned to $^2H_{11/2} \rightarrow {}^4I_{15/2}$ and $^4S_{3/2} \rightarrow {}^4I_{15/2}$ transition, respectively. The extremely weak red emission peak at 659 nm corresponds to the $^4F_{9/2} \rightarrow {}^4I_{15/2}$ transition. The co-doped $NaLuF_4$:Yb^{3+}/Er^{3+} system exhibits green light to naked eyes as a whole (Fig. 4d). According to Auzel's theory, the upconversion emission intensity (I) is related to the excitation power (P), that can expressed by the equation $I \propto P^n$, where n is the number of the absorbed infrared photons for emitting a visible photon.[37] Both green and blue emission usually involve in a two-photon upconversion process (n=2), since the excitation energy of an infrared photon is inadequate for generating one visible emission photon.[5]

To obtain the multicolor output from yellow-green to red emission in visible region, the UC emission of $NaLuF_4$:Yb^{3+},Er^{3+} nanocrystals is tuned by controlling the dopant concentration of Yb^{3+} ion. In Fig. 3, four common emission peaks centered at 411 nm, 529 nm, 541 nm and 657 nm are observed which are assigned to $^4F_{5/2} \rightarrow {}^4I_{15/2}$, $^2H_{11/2}$,$^4S_{3/2} \rightarrow {}^4I_{15/2}$ and $^4F_{9/2} \rightarrow {}^4I_{15/2}$ transition of Er^{3+}, respectively. Noticeably, it can be seen that the relative intensity of red to green emission gradually increases with increasing the concentration of Yb^{3+} ion from 30 mol% to 90 mol%. There are mainly two reasons leading to this variation.

First, the energy transfer rate from Yb^{3+} to Er^{3+} will be improved with increasing the content of Yb^{3+} ion under the excitation of 980 nm infrared power which can be theoretically explained according to Dexter's formulation as following:[38]

$$P(R) \propto \frac{Q_A}{R^b \tau_D} \int \frac{f_D(E) F_A(E)}{E^c} dE \qquad (1)$$

where Q_A is the total absorption cross section of the acceptor ion, R represents the distance between the donor ion and the acceptor ion, τ_D is the decay time of the donor emission, b and c are the parameters

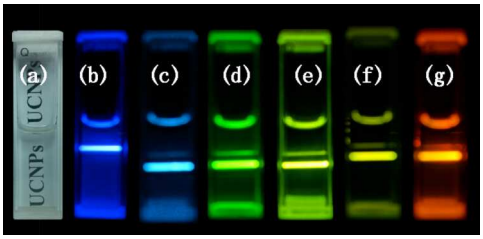

Fig. 4 (a) Bright-field photo of the prepared $NaLuF_4$ nanocrystals dispersed in cyclohexane. Eye-visible luminescence photos of the colloidal solution of $NaLuF_4$ doped with (b) 18%Yb^{3+}/0.5%Tm^{3+}; (c) 18%Yb^{3+}/0.04%Er^{3+}/0.7%Tm^{3+}, (d) 18%Yb^{3+}/2%Er^{3+}, and (e-g) (30,32,90)%Yb^{3+}/1%Er^{3+} under the excitation of a 980 nm laser diode.

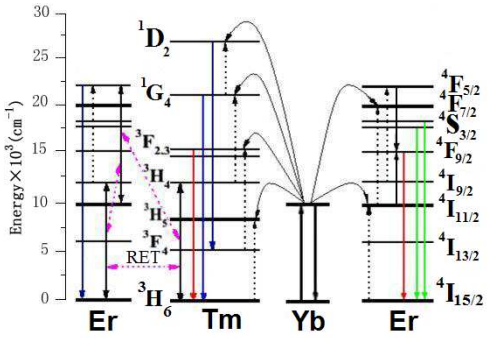

Fig. 5 Schematic energy level diagram of upconversion excitation and emission processes and the reversible energy transfer between Er^{3+} and Tm^{3+}.

dependent on energy transfer type, and the function $f_D(E)$ and $F_A(E)$ represent the observed shapes of the donor emission band and the acceptor absorption band, respectively. It can be seen in equation that the energy transfer rate $P(R,\tau_D)$ is in inverse proportion to the distance R between donors and acceptors. In our work, the distance R between Yb^{3+} and Er^{3+} decreased owing to the elevated Yb^{3+} concentration in host lattice, then, the energy transfer rate $P(R)$ from Yb^{3+} to Er^{3+} will be accelerated correspondingly according to equation (1) when other variables are kept the same. The enhanced energy transfer rate mainly leads to the increase of populating electrons in $^4F_{7/2}$ and $^4I_{11/2}$ energy levels. As a result, the populating electrons in the red level ($^4F_{9/2}$) of Er^{3+} ion will be largely increased by the $4f^n$-shell electronic transition $^4F_{7/2}+^4I_{11/2}\rightarrow 2*^4F_{9/2}$ (Fig. 5).

Second, when increasing the dopant concentration of Yb^{3+} ion in the heavy doping level, concentration quenching effect will dominate the upconversion emission and leads to the decrease of both green and red emission bands of Er^{3+} ion. However, it should be noted that concentration quenching effect has different impact on red and green emission. On the condition of heavy doping with Yb^{3+} ion, most of the irradiation energy from Yb^{3+} ion will be consumed by the thermal vibration of crystal lattice, so that the electronic population of Er^{3+}-$^4F_{7/2}$ level is obviously decreased. On the other hand, the green light levels ($^4S_{3/2}$/$^2H_{11/2}$) of Er^{3+} are predominantly depopulated by the upper $^4F_{7/2}$ level. Thus, the decrease of the electronic population in $4F_{7/2}$ level directly leads to the decrease of the electronic population in $^4S_{3/2}$/$^2H_{11/2}$ levels. Different from the relatively homogeneous population path of green light level ($^4S_{3/2}$/$^2H_{11/2}$), the red light level ($^4F_{9/2}$) has more adequate populating routes. It is not only depopulated by the upper $^4F_{7/2}$ level and affected by the population of $^4F_{7/2}$ level, but also simultaneously populated by other more efficient route $^4F_{7/2}+^4I_{11/2}\rightarrow 2*^4F_{9/2}$. As a result, the heavy doping of Yb^{3+} ion decreases the green emission more than the red emission of Er^{3+} ion due to the concentration quenching effect. Of course, this presents a relative increase of red to green emission on the fluorescent spectra.

3.2 Plant cell imaging

Conventional bio-slice imaging technology has been gradually substituted by fluorescent imaging in biological and clinical application due to its defects of complicated slicing process and strictly limited thickness, which is restricted to the bio-imaging in vitro. The fluorescent bio-imaging is recently renovated and developed based on the upconversion nanoparticles. The imaging

mechanism of upconversion fluorescent imaging is completely different from the bio-slice imaging, where the upconversion fluorescence imaging was accomplished by collecting the reflected fluorescent signal from the tissues in vivo or in vitro while the transmitted light through the flimsy tissue with slicing process was collected for conventional imaging in vitro. Moreover, upconversion fluorescent imaging employs infrared light as excitation source, which has higher temporal and spatial resolution, absence of auto-fluorescence, and higher penetration depth in tissues (up to 3.2 cm) than the visible light source employed in the conventional slice imaing.[39] Due to these advantages, upconversion fluorescent labels have great potential application in the field of biological imaging in vivo and in vitro.

In our work, fluorescence imaging technique was used for imaging the onion epidermal cells. However, in order to conveniently compare with conventional bio-slice imaging by way of collecting transmitted light under condition of controlling other various factors, the onion slices was adopted as research objectives for fluorescence imaging, but the living onion without need of slicing process can be used directly for fluorescence imaging in vivo in practical biological applications.

In order to confirm the feasibility of upconversion nanoprobes, the multicolor bioimaging is conducted on onion epidermal cells incubated with $NaLuF_4$ nanocrystals. First, the onion epidermal slices were dried at temperature of 35 °C for one day. Second, an aqueous dispersion of UCNPs was added to container with onion epidermal slices, which were incubated for 15 min at 26 °C. The cell imaging was measured by a confocal fluorescence microscopy (Olympus BX43) equipped with a 980 nm NIR diode laser after incubated with different kinds of $NaLuF_4$ nanocrystal aqueous solution. The fluorescent images of the onion epidermal cells with upconversion nanoprobes are shown in Fig. 6 for comparing with conventional slicing imaging. It can be seen clearly in Fig. 6a that the onion epidermal cells exhibited eye-visible blue UC luminescence. In addition, unambiguous cell structure is observed with assistance of UC fluorescence. The shape and position of the cells overlapped very well in

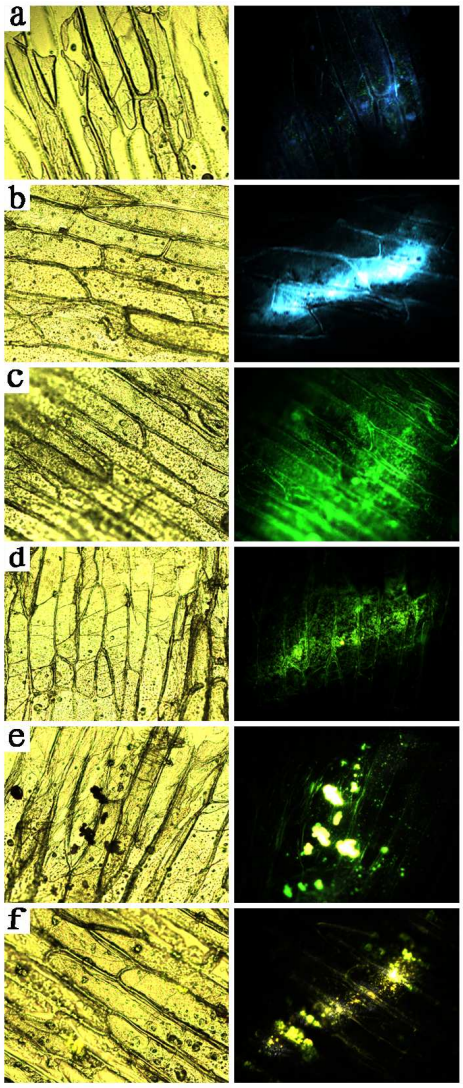

Fig. 6 Right column: Fluorescence microscope imaging of onion epidermal slices under the excitation of a 980 nm laser diode loaded with $NaLuF_4$ nanocrystals doped with (a) 18%Yb^{3+}/0.5%Tm^{3+}; (b) 18%Yb^{3+}/0.04%Er^{3+}/0.7%Tm^{3+}; (c) 18%Yb^{3+}/2%Er^{3+}; and (d-f) (30,32,90%)Yb^{3+}/1%Er^{3+}. **Left column:** conventional slice transmission imaging. Enlarged by 100×.

bright field and dark field, which indicated well biocompatibility between $NaLuF_4$ nanocrystals and onion epidermal cells. Importantly, the cell wall and cytoplasm can be specifically distinguished by the chiseled fluorescent imaging, since they have different biocompatibility to upconversion nanoprobes. To change the multicolor upconversion nanoprobes, cyan, green, olivine, yellow, and red images of onion epidermal cells can be obtained which were shown in Fig. 6b-6f.

Conventional transmission imaging (left column in Fig. 6) and upconversion fluorescent imaging (right column in Fig. 6) are both capable of presenting the microstructure of slicing cells in vitro. However, the conventional slicing transmission imaging is incapable of presenting the cell microstructures in vivo. We chose a complete and living onion which is loaded with upconversion nanoprobes in the surface cells by drying and immersing procedures. It can be observed from Fig. 7 that upconversion fluorescent nanoprobes can show clearly the cell microstructures (right column in Fig. 7) in vivo, while the conventional transmission imaging has no optical signals (left column in Fig. 7) since it is just suitable for imaging ultrathin slices.

3.3 Detection of sodium fluorescein

Sodium fluorescein is a kind of organic dye which is widely applied as the injection for clinical diagnosis of the cornea, which is almost harmless to human being if correctly controlling the doses.

Here, we show that upconversion fluorescent nanoprobes is very efficient and viable for detecting sodium fluorescein in vitro or in vivo, based on a luminescent resonance energy transfer process from UCNPs to sodium fluorescein. The detection limitation can reach to 0.14 μg/ml in solution or 0.14 $\mu g/cm^3$ in living organisms. More

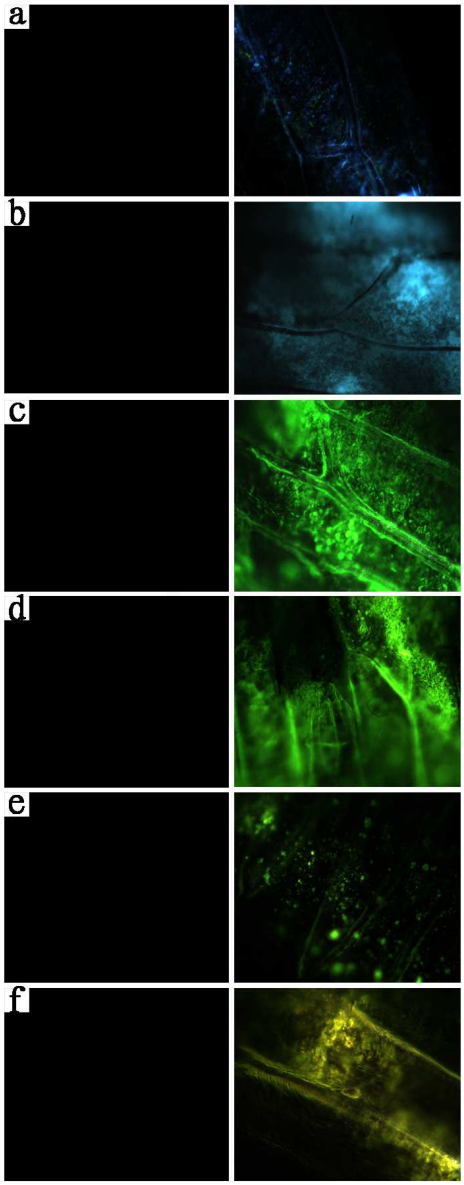

Fig. 7 Right column: Fluorescence microscope imaging of a complete and living onion under the excitation of a 980 nm laser diode loaded with $NaLuF_4$ nanocrystals doped with (a) 18%Yb^{3+}/0.5%Tm^{3+}; (b) 18%Yb^{3+}/0.04%Er^{3+}/0.7%Tm^{3+}; (c) 18%Yb^{3+}/2%Er^{3+}; and (d-f) (30,32,90%)Yb^{3+}/1%Er^{3+}. **Left column:** conventional transmission imaging without detectable optical signal. Enlarged by 500×.

importantly, the detection sensitivity of these LRET based nanoprobes is higher by several orders of magnitude than that of conventional approach where the blue pump power is directly applied for detecting sodium fluorescein. Furthermore, the merits of these LRET based nanoprobes include deeper

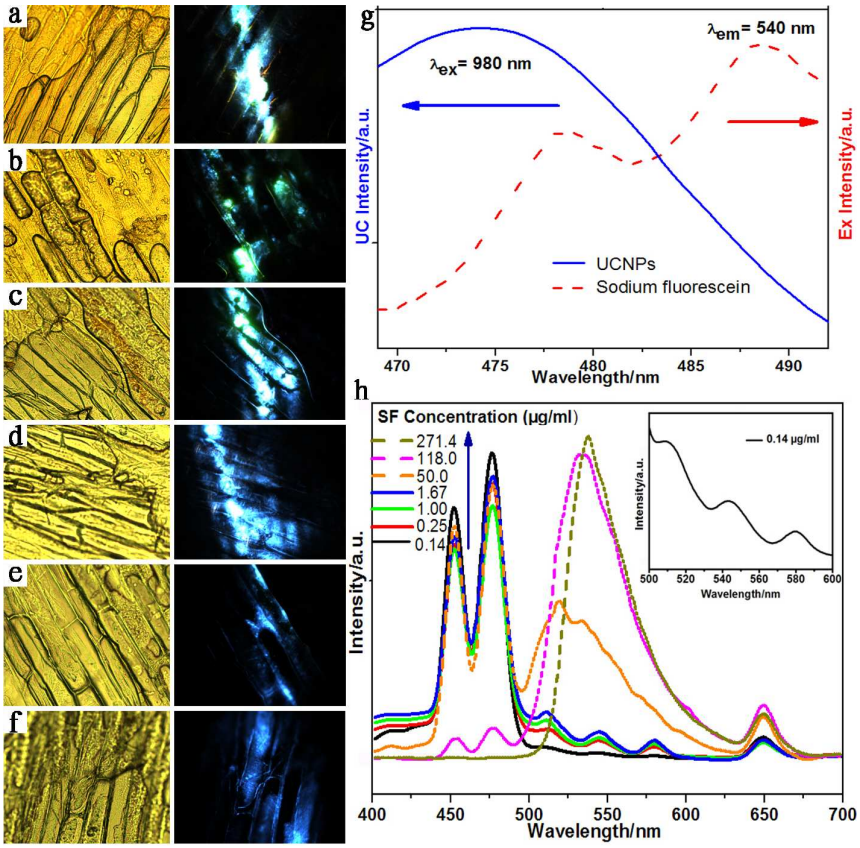

Fig. 8 Right column: fluorescence microscope imaging of onion epidermal cells after incubated with $NaLuF_4$: 18%Yb^{3+},0.5%Tm^{3+}@SF for 15 min. Concentration of $NaLuF_4$ nanocrystals equals to 16.5 mg/ml, that of SF equals to (a) 5 μg/ml, (b) 2.5 μg/ml, (c) 1.25 μg/ml, (d) 0.625 μg/ml, (e) 0.3125 μg/ml, (f) 0 μg/ml. **Left column:** conventional slice transmission imaging. Enlarged by 100×. (g) The UC fluorescence spectrum of $NaLuF_4$:18%Yb^{3+},0.5%Tm^{3+} nanocrystals (λ_{ex}=980 nm) and excitation spectrum of sodium fluorescein (λ_{em}=540 nm). (h) Evolution of the fluorescence of UCNPs@SF with different concentration of SF (from 0.14 to 271.4 μg/ml) under the excitation of 980 nm laser. Insert of (h): The corresponding magnification of the UCL spectra of UCNPs@SF between 500 nm and 600 nm when concentration of SF equals to 0.14 μg/ml.

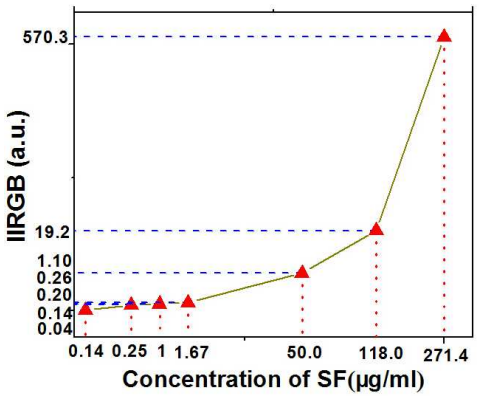

Fig. 9 The curves of Integral Intensity Ratio of Green to Blue (IIRGB) VS concentration of SF.

penetration depth of the infrared excitation light, background-free imaging, and high signal to noise ratios.

There is a perfect overlap between the excitation spectra of sodium fluorescein and the emission spectra of $NaLuF_4$:18%Yb^{3+}/0.5%Tm^{3+} nanoparticles in blue region, so that an LRET based sensor system can be successfully constructed by combining the UCNPs with sodium fluorescein, in which UCNPs play a role of energy donor and sodium fluorescein plays a role of energy acceptor. It is clear from Fig. 8g that the excitation peak of SF solution located at 479 nm. Meanwhile, it is observed that the UC emission of $NaLuF_4$ nanoparticles (donors) centered at 474 nm, which has large overlap area with the excitation peaks of sodium fluorescein (acceptor). The UC fluorescent nanoprobes with an acidic ligand (OA) can quickly capture the basic sodium fluorescein

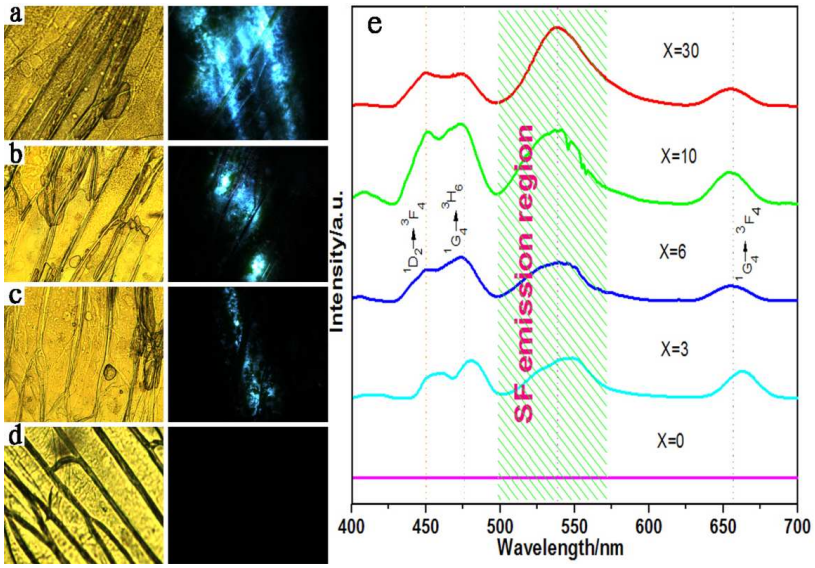

Fig. 10 Right column: Fluorescence microscope imaging of onion epidermal cells after incubated with $NaLuF_4$:18%Yb^{3+}/0.5% Tm^{3+}@ SF. Concentration of SF equals to 2.5 μg/ml, that of $NaLuF_4$ nanocrystals equals to (a) 30 mg/ml, (b)10 mg/ml, (c) 6 mg/ml, and (d) 0 mg/ml. **Left column:** conventional slice transmission imaging. Enlarged by 100×. (e) Evolution of the fluorescence spectra of UCNPs@SF in the presence of various concentrations of UCNPs (from 0 to 30 mg/ml) in cyclohexane.

in plant cells and forms a close UCNPs@SF system. It is clear from the right column in Fig. 8a-c that UCNPs@SF system can emit cyan light under the excitation of 980 nm infrared light which is actually composed of the blue emission of $NaLuF_4$:18%Yb^{3+}/0.5%Tm^{3+} nanoparticles and green emission of sodium fluorescein. This simultaneously indicates the occurrence of the efficient LRET process.

The fluorescence imaging of onion epidermal cells with UCNPs@SF are depicted in right column of Fig. 8a-f, where concentration of sodium fluorescein is decreased from 5 to 0 μg/ml. The fluorescence imaging was collected by a confocal fluorescence microscopy equipped with a 980 nm diode laser as the excitation source. It is clearly observed that the onion epidermal cell cytoskeleton with sodium fluorescein more than 0.625 μg/ml exhibited bright cyan light to naked eyes. Decreasing the concentration of sodium fluorescein from 5 to 0 μg/ml, the obvious emission color on the cells gradually varied from cyan color emission to blue color emission without attenuation of comprehensive luminescence intensity.

Figure 8d shows that blue emission dominates the overall fluorescence due to the relative weaker green emission from sodium fluorescein. When decreasing the concentration of sodium fluorescein further to 0, it can be seen in right Fig. 8f that the onion epidermal cells exhibited pure blue color fluorescence without cyan color emission. The corresponding UC luminescence spectra of UCNPs@SF system with various concentration of sodium fluorescein solution were also investigated in Fig. 8h. There are main peaks located at ~477 nm，~650 nm and ~537 nm in upconversion fluorescent spectra, which are ascribed to the $^1G_4 \rightarrow {}^3H_6$, $^3F_{2,3} \rightarrow {}^3H_6$ transition of Tm^{3+} and exciton recombination radiation in sodium fluorescein achieved by LRET from $NaLuF_4$ nanoparticles (Donors) to sodium fluorescein (Acceptors) in the onion epidermal cells under 980 nm laser excitation. The red shift of the emission peaks of SF were due to two main reasons: first, dipolymer and polymer were developed by polymerization

with increasing the concentration of SF, excitation energy of the first electronic singlet state of them is lower than that of monomer, as a result, there existed a red shift for emission wavelength; second, when adding the SF aqueous solution, polarity of the solvent was enhanced owing to the elevated amount of water, the fluorescence emission was gradually substituted by relaxation state emission, which is the other reason for red shift.

The three emission peaks centered at ~510 nm, ~540 nm, and ~580 nm are assigned to emission of three different isomers of sodium fluorecein when value of solution PH is about 7. Alkalinity of the whole solution is enhanced when increasing the concentration of SF. As a result, there is only one form of SF in solution, corresponding to one emission peak. The peak at around 650nm originated from the $^3F_{2,3}$-$^3H_6$ transition of Tm^{3+} ions. In addition, it can be seen from Fig. 8h that the green emission center at 537 nm increases relative to the blue emission centered at 477 nm with increasing the concentration of sodium fluorescein. Importantly, the integral intensity ratio of green to blue emission (IIRGB) can vary in a large range as shown in Fig. 9. E.g., the UCNPs@SF system with 0.14 μg/ml has a IIRGB value of 0.04 while the one with 271.4 μg/ml has a IIRGB value of 570.3. The concentration of sodium fluorescein can be easily addressed according to IIRGB signal. The wide range of IIRGB values is beneficial to the quick and precise detection of sodium fluorescein concentration. Employing a 980 nm-diode infrared power source of 0.2 W/mm^2, the detection limitation of sodium fluorescein can reach to 0.14 ug/cm^3 in living onion cells if the concentration of upconversion nanoprobes is properly controlled.

The concentration of $NaLuF_4$ upconversion nanoprobes has also remarkable influence on the detection precision of UCNPs@SF system. The fluorescent imaging of onion epidermal cells with UCNPs@SF was depicted in the right column of Fig. 10a-d, of which the emission intensity decrease with decreasing the concentration of upconversion nanoprobes. Noticeably, it is observed from Fig. 10d that no fluorescence was detected which strongly supports that the green emission of sodium fluorescein is excited by the blue light from $NaLuF_4:Yb^{3+}/Tm^{3+}$ upconversion nanoprobes.

UC fluorescent spectra of UCNPs@SF with various concentrations of $NaLuF_4$ nanoparticles are shown in Fig. 10e. All luminescent spectra present four peaks centered at 449 nm/474 nm/655 nm (Tm) and ~538 nm (UCNPs@SF) except the one without upconversion nanoprobes. The three peaks of upconversion nanoprobes were attributed easily to $^1D_2 \rightarrow {}^3F_4$, $^1G_4 \rightarrow {}^3H_6$ and $^1G_4 \rightarrow {}^3F_4$ transition of Tm^{3+}, while the emission peak centered at 538 nm is ascribed to the emission of sodium fluorescein by LRET between UCNPs and SF. Especially, it can be noted readily that a redshift occurs with decreasing the concentration of upconversion nanoprobes from 30 to 3 mg/ml. Unexpectedly, the IIRGB value is independent on the concentration of upconversion nanoprobes if fixing the concentration of SF.

4. Conclusion

In conclusion, $NaLuF_4$ upconversion fluorescent nanoprobes with doping were successfully synthesized via the solvothermal method, of which multicolor emission can be efficiently tuned from blue to red under the excitation of a single wavelength infrared light source. There UC fluorescent nanoprobes were subsequently used for imaging the onion epidermal cells and detecting sodium fluorescein in plant cells. For direct fluorescent imaging in vivo, a complete and

living onion is loaded with upconversion nanoprobes in the surface cells by drying and immersing procedures. The measured fluorescent images in a confocal fluorescence microscopy indicates that these UC fluorescent nanoprobes can show clearly the cell microstructures in vivo, while the conventional transmission imaging has no detectable optical signals since it is just suitable for imaging ultrathin slices.

Detecting sodium fluorescein in plant cells is based on a LRET process from UCNPs to SF. The UC fluorescent nanoprobes with an acidic ligand can quickly capture the basic sodium fluorescein in plant cells and forms a close UCNPs@SF system. The measured fluorescent images indicate that UCNPs@SF system can emit cyan light under the excitation of 980 nm infrared light which is actually composed of the blue emission of $NaLuF_4$:18%Yb^{3+}/0.5%Tm^{3+} nanoprobes and green emission of SF. The concentration of SF can be easily addressed according to IIRGB signal. The wide range of IIRGB values is beneficial to the quick and precise detection of SF concentration. Employing a 980 nm-diode infrared power source of 0.2 W/mm^2, the detection limitation of SF can reach to 0.14 ug/cm^3 in living onion cells if the concentration of upconversion nanoprobes is properly controlled. Unexpectedly, the IIRGB value is independent on the concentration of upconversion nanoprobes if fixing the concentration of SF.

This procedure based on LRET process opens a novel route for detecting sodium fluorescein in living organisms and the clinical diagnosis of the cornea.

Acknowledgements

Financial support from the National Natural Scientific Foundation of China (21301058 and 61274026)

Notes and References

1 M. Schuelke, *Nat. Biotechnol.*, 2000, **18**, 233.

2 M. P. Robin, P. Wilson, A. B. Mabire, J. K. Kiviaho, J. E. Raymond, D. M. Haddleton and R. K. O. Reilly, *J. Am. Chem. Soc.*, 2013, **135**, 2875.

3 J. C. Bigge, T. P. Patel, J. A. Bruce, P. N. Goulding, S. M. Charles and R. B. Parekh, *Anal. Biochem.*, 1995, **230**, 229.

4 D. Riccardi, P. Schaefer, Y. Yang, H. B. Yu, N. Ghosh, X. Prat-Resina, P. Ko1nig, G. H. Li, D. G. Xu, H. Guo, M. Elstner and Q. Cui, *J. Phys. Chem. B*, 2006, **110**, 6458.

5 F. Wang, D. Banerjee, Y. S. Liu, X. Y. Chen and X. G. Liu, *Analyst*, 2010, **135**, 1839.

6 J. G. White, W. B. Amos and M. Fordham, *J. Cell Biol.*, 1987, **105**, 41.

7 P. K. Jain, K. S. Lee, I. H. El-Sayed and M. A. El-Sayed, *J. Phys. Chem. B*, 2006, **110**, 7238.

8 H. Li and L. Y. Wang, *Analyst*, 2013, **138**, 1589.

9 Q. Liu, J. J. Peng, L. N. Sun and F. Y. Li, *ACS Nano*, 2011, **5**, 8040.

10 L. Q. Xiong, Z. G. Chen, M. X. Yu, F. Y. Li, C. Liu, C. H. Huang, *Biomaterials*, 2009, **30**, 5592.

11 L. Cheng, K. Yang, Y. G. Li, J. H. Chen, C. Wang, M. W. Shao, S. T. Lee and Z. Liu, *Angew. Chem.*, 2011, **123**, 7523.

12 C. X. Li, Z. Y. Hou, Y. L. Dai, D. M. Yang, Z. Y. Cheng, P. A. Ma and J. Lin, *Biomater. Science*, 2013, **1**, 213.

13 G. B. Shan, R. Weissleder and S. A. Hilderbrand, *Theranostics*, 2013, **3**, 276.

14 M. De, S. Rana, H. Akpinar, O. R. Miranda, R. R. Arvizo, U. H. F. Bunz and V. M. Rotello, *Nature Chem.*, 2009, **1**, 461.

15 C. Röcker, M. Pötz, F. Zhang, W. J. Parak and G. U. Nienhaus, *Nature Nanotech.*, 2009, **4**, 577.

16 L. Cheng, K. Yang, M. W. Shao, S. T. Lee and Z. Liu, *J. Phys. Chem. C*, 2011, **115**, 2686.

17 M. Wang, C. C. Mi, W. X. Wang, C. H. Liu, Y. F. Wu, Z. R. Xu, C. B. Mao and S. K. Xu, *ACS Nano*, 2009, **3**, 1580.

18 M. D. Garrett, A. D. Dukes, J. R. McBride, N. J. Smith, S. J. Pennycook and S. J. Rosenthal, *J. Phys. Chem. C*, 2008, **112**, 12736.

19 A. M. Saad, M. B. Mohamed, M. T. H. A. Kana, I. M. Azzouz, *Opt. Laser Technol.*, 2013, **46**, 1.

20 J. C. Boyera and F. C. J. M. V. Veggel, *Nanoscale*, 2010, **2**, 1417.

21 M. Y. Berezin and S. Achilefu, *Chem. Rev*., 2010, **110**, 2641.

22 L. Q. Xionga, T. S. Yanga, Y. Yanga, C. J. Xub, F. Y. Li, *Biomaterials,* 2010, **31**, 7078.

23 G. Tian, Z. J. Gu, L. J. Zhou, W. Y. Yin, X. X. Liu, L. Yan, S. Jin, W. L. Ren, G. M. Xing, S. J. Li and Y. L. Zhao, *Adv. Mater.*, 2012, **24**, 1226.

24 H. Kobayashi, N. Kosaka, M. Ogawa, N. Y. Morgan, P. D. Smith, C. B. Murray, X. C. Ye, J. Collins, G. A. Kumar, H. Bell and P. L. Choyke, *J. Mater. Chem.*, 2009, **19**, 6481.

25 F. Wang and X. G. Liu, *Acc. Chem. Res.*, 2014, **47**, 1378.

26 S. Haacke, R. A. Taylor, I. B. Joseph, M. J. S. P. Brasil, M. Hartig and B. Deveaud, *JOSA B*, 1998, **15**, 1410.

27 Y. H. Chen, J. Z. Zhao, H. M. Guo and L. J. Xie, *J. Org. Chem.*, 2012, **77**, 2192.

28 Y. X. Liu, D. S. Wang, J. X. Shi, Q. Peng and Yadong Li, *Angew. Chem. Int. Ed.*, 2013, **52**, 4366.

29 D. R. Larson, W. R. Zipfe, R. M. Williams, S. W. Clark, M. P. Bruchez, F. W. Wise, W. W. Webb, *Science*, 2003, **300**, 1434.

30 Y. Sun, M. X. Yu, S. Liang, Y. J. Zhang, C. G. Li, T. T. Mou, W. J. Yang, X. Z. Zhang, B. Li, C. H. Huang and F. Y. Li, *Biomaterials*, 2011, **32**, 2999.

31 Z. Q. Li, Y. Zhang and S. Jiang, *Adv. Mater.*, 2008, **20**, 4765.

32 N. S. Allen and D. T. Brown, *Cell Motil. Cytoskel.*, 1988, **10**, 153.

33 M. L. Winter, M. D. Ellis, W. R. Snodgrass, *Ann. Emerg. Med.*, 1990, **19**, 663.

34 X. Z. Xiao, G. Z. Lua, S. D. Shen, D. S. Mao, Y. Guo and Y. Q. Wang, *Mater. Sci. Eng., B*, 2011, **176,** 72.

35 P. Zhang, S. Rogelj, K. Nguyen and D. Wheeler, *J. Am. Chem. Soc.*, 2006, **128**, 12410.

36 R. D. Shannon, *Acta. Cryst.,* 1976. **A32**, 751.

37 M. Pollnau, D. R. Gamelin, S. R. Luthi, H. U. Gudel and M. P. Hehlen, *Phys. Rev. B,* 2000, **61**, 3337.

38 D. J. Dexter, *J. Chem. Phys.,* 1953, **21**, 836.

39 G. Y. Chen, J. Shen, T. Y. Ohulchanskyy, N. J. Patel, A. Kutikov, Z. P. Li, J. Song, R. K. Pandey, H. Ågren, P. N. Prasad and G. Han, *ACS Nano*, 2012, **6**, 8280.

TOC

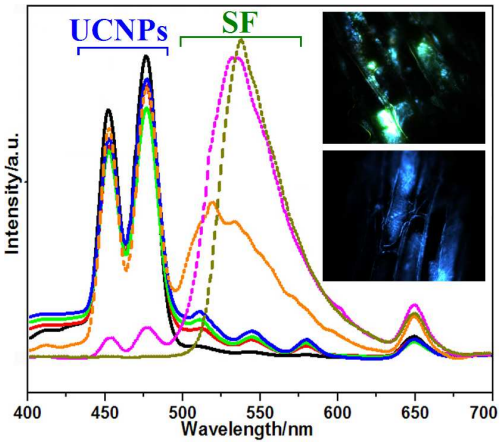

Detection limitation of sodium fluorescein in plant cells can reach to 0.14 μg/cm^3 based on LRET from UCNPs to SF .